Journal of Virology®

VIRUS-CELL INTERACTIONS

Glycine 29 Is Critical for Conformational Changes of the Spike Glycoprotein of Mouse Hepatitis Virus A59 Triggered by either Receptor Binding or High pH

Dan Mi,[a] Xiuyuan Ou,[a] Pei Li,[a] Guiqing Peng,[b] Yan Liu,[a] Ruixuan Guo,[a] Zhixia Mu,[a] Fang Li,[c] Kathryn Holmes,[d] Zhaohui Qian[a]

[a]NHC Key Laboratory of Systems Biology of Pathogens, Institute of Pathogen Biology, Chinese Academy of Medical Sciences and Peking Union Medical College, Beijing, China

[b]State Key Laboratory of Agricultural Microbiology, College of Veterinary Medicine, Huazhong Agricultural University, Wuhan, China

[c]Department of Pharmacology, University of Minnesota Medical School, Minneapolis, Minnesota, USA

[d]Department of Microbiology, University of Colorado School of Medicine, Aurora, Colorado, USA

ABSTRACT Mouse hepatitis virus (MHV) uses its N-terminal domain (NTD) of the viral spike (S) protein to bind the host receptor mouse carcinoembryonic antigen-related cell adhesion molecule 1a (mCEACAM1a) and mediate virus entry. Our previous crystal structure study of the MHV NTD/mCEACAM1a complex (G. Peng, D. Sun, K. R. Rajashankar, Z. Qian, et al., Proc Natl Acad Sci U S A 108:10696–10701, 2011, https://doi.org/10.1073/pnas.1104306108) reveals that there are 14 residues in the NTD interacting with the receptor. However, their contribution to receptor binding and virus entry has not been fully investigated. Here we analyzed 13 out of 14 contact residues by mutagenesis and identified I22 as being essential for receptor binding and virus entry. Unexpectedly, we found that G29 was critical for the conformational changes of the S protein triggered by either receptor binding or high pH. Replacement of G29 with A, D, F, K, M, and T, to different extents, caused spontaneous dissociation of S1 from the S protein, resulting in an enhancement of high-pH-triggered receptor-independent syncytium (RIS) formation in HEK293T cells, compared to the wild type (WT). In contrast, replacement of G29 with P, a turn-prone residue with a strict conformation, hindered virus entry and conformational changes of the S protein triggered by either receptor binding or pH 8.0, suggesting that the structural turn around G29 and its flexibility are critical. Finally, stabilization of the NTD by G29P had almost no effect on pH-independent RIS induced by the Y320A mutation in the C-terminal domain (CTD) of the S1 subunit, indicating that there might be an absence of cross talk between the NTD and CTD during conformational changes of the S protein. Our study will aid in better understanding the mechanism of how conformational changes of the S protein are triggered.

IMPORTANCE Binding of the MHV S protein to the receptor mCEACAM1a triggers conformational changes of S proteins, leading to the formation of a six-helix bundle and viral and cellular membrane fusion. However, the mechanism by which the conformational change of the S protein is initiated after receptor binding has not been determined. In this study, we showed that while replacement of G29, a residue at the edge of the receptor binding interface and the center of the structural turn after the β1-sheet of the S protein, with D or T triggered spontaneous conformational changes of the S protein and pH-independent RIS, the G29P mutation significantly impeded the conformational changes of S proteins triggered by either receptor binding or pH 8.0. We reason that this structural turn might be critical for conformational changes of the S protein and that altering this structural turn could initiate conformational changes of the S protein, leading to membrane fusion.

Citation Mi D, Ou X, Li P, Peng G, Liu Y, Guo R, Mu Z, Li F, Holmes K, Qian Z. 2019. Glycine 29 is critical for conformational changes of the spike glycoprotein of mouse hepatitis virus A59 triggered by either receptor binding or high pH. J Virol 93:e01046-19. https://doi.org/10.1128/JVI.01046-19.

Editor Tom Gallagher, Loyola University Chicago

Address correspondence to Zhaohui Qian, zqian2013@sina.com.

D.M. and X.O. contributed equally to this work.

Received 24 June 2019
Accepted 19 July 2019
Accepted manuscript posted online 2 August 2019
Published 30 September 2019

KEYWORDS mouse hepatitis virus, S protein conformational change, coronavirus spike glycoprotein, initiation of conformational change, receptor-independent syncytium formation

Coronaviruses (CoVs) are a large family of enveloped plus-stranded RNA viruses that infect humans and animals and cause a variety of diseases, including respiratory, enteric, hepatic, and neurotropic diseases (1). Phylogenetically, CoVs are classified into four genera, alphacoronaviruses, betacoronaviruses, gammacoronaviruses, and deltacoronaviruses (2). Mouse hepatitis virus (MHV) is a lineage A betacoronavirus and is commonly used as a model to study CoV entry, replication, and pathogenesis. MHV utilizes murine carcinoembryonic antigen-related cell adhesion molecule 1 (mCEACAM1) as a receptor (3, 4). CEACAM1 is an immunoglobulin superfamily (IgSF) member and is involved in various functions, including development, angiogenesis, tumorigenesis, and innate and adaptive immune responses, etc. (5). There are two alleles of the CEACMA1 gene in mouse populations: mCEACAM1a and mCEACAM1b. Although they share 75% identity in the N-terminal Ig-like domain where the MHV spike (S) protein binds, only mCEACAM1a is an effective receptor for MHV (4, 6, 7). Several critical contact residues for MHV S protein binding are missing in mCEACAM1b, including the critical isoleucine 41 (I41) and arginine 47 (R47) residues (7).

The entry of CoV is mediated by the interaction between the receptor and the viral S protein. The S protein is a member of the class I viral fusion proteins. Each monomer of the trimeric S protein is about 180 to 200 kDa and composed of two subunits, S1 and S2. Like most other class I viral fusion proteins, S1 contains the receptor binding domain (RBD), while S2 possesses the fusion machinery, including the fusion peptide, two heptad repeats (HRs), the juxtamembrane domain, and the transmembrane domain (Fig. 1A) (8–12). Cleavage between S1 and S2 is critical for S protein-mediated cell-cell fusion (also called syncytium formation) (13), and an additional cleavage(s) prior to the fusion peptide is required for virus entry (12, 14, 15). S1 can be further divided into two subdomains: the N-terminal domain (NTD) and the C-terminal domain (CTD). Depending on the specific coronavirus, the RBD can be located in either the NTD or CTD (Fig. 1A). While RBDs of all known alphacoronaviruses and most of the known betacoronaviruses are located in the CTD (16–22), MHV uses its NTD to bind mCEACAM1a (23). Our previous structural studies on the NTD/mCEACAM1a complex revealed that the MHV NTD folds like human galectins and that 14 residues on the NTD make direct contacts with mCEACAM1a (Fig. 1B). However, the contribution of each individual contacting residue in the NTD to receptor binding and virus entry has not been fully analyzed. In this study, we systematically investigated the role of most contacting residues of NTDs in receptor binding and infection and found that R20, I22, N26, and N172 are critical for receptor binding and virus entry. Surprisingly, we found that G29 was critical for conformational changes of the S protein, although it had no influence on receptor binding.

RESULTS

There are 14 residues in the NTD of the MHV-A59 S protein making direct contact with mCEACAM1a (Fig. 1B) (24). To evaluate their individual contributions to the binding of mCEACAM1a, we mutated each of these contact residues in the S protein to alanine or the corresponding residues (R20K and G29D) in the S protein of bovine CoV based on the alignment, except for phenylalanine 19 (F19). We first determined if any of the mutations had any effect on S protein expression and processing. The plasmids carrying individual mutant S genes were transfected into HEK293T cells, and their expression was analyzed by Western blotting. In agreement with our previous reports (12), there are two major species of S proteins detected by Western blotting using polyclonal goat anti-MHV S antibody AO4, the full-length S protein of around 180 kDa and a cleaved S protein of around 90 kDa (Fig. 1C). All of the mutant S proteins were expressed in HEK293T cells at levels similar to those of the wild type (WT), indicating

A

B

MHV S	Y15	F19	R20	I22	Q23	L24	V25	N26	S27	G29	L89	L160	N172	L174
mCEACAM1a	I41 D42	N94	Y34 T39 R96	G29 A30 V49	R47	M54 F56	R47 F56	F56 T57	T57 G58 Q59	Q59	I41 D42 Q59	I41	V49 N51 S52	E93

C

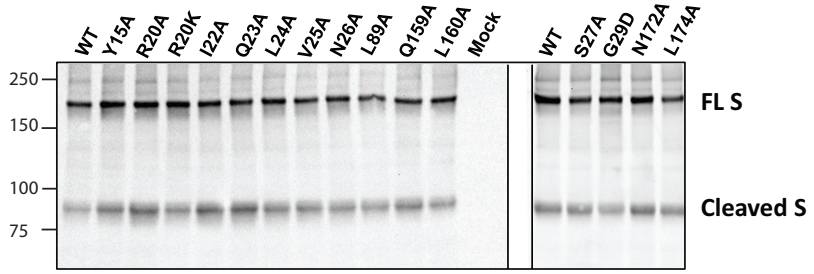

D

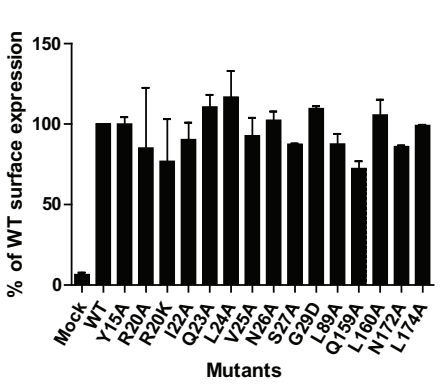

E

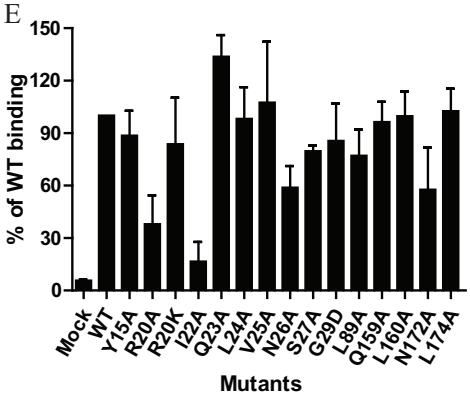

FIG 1 Analysis of expression and receptor binding of mutant MHV S proteins in HEK293T cells. (A) Schematic diagram of the MHV-A59 S protein. NTD, N-terminal domain; CTD, C-terminal domain; FP, fusion peptide; HR-N, N-terminal heptad repeat; HR-C, C-terminal heptad repeat; JMD, juxtamembrane domain; TMD, transmembrane domain. (B) Amino acid residues at the NTD/mCEACAM1a interface. (C) Expression of WT or mutant MHV S proteins in HEK293T cell lysates. The full-length (FL) (about 180 kDa) and cleaved (about 90 kDa) S proteins of MHV-A59 were detected by using goat anti-MHV S antibody AO4. (D) Flow cytometry analysis of surface expression of mutant MHV-A59 S proteins on HEK293T cells. HEK293T cells transiently expressing mutant S proteins were stained with polyclonal goat anti-MHV S antibody AO4. The amount of WT S protein on the cell surface was set to 100%. All of the experiments shown were repeated at least three times. Data are shown as means with standard deviations. (E) Analysis of receptor binding activities of WT and mutant S proteins by flow cytometry. HEK293T cells transiently expressing mutant MHV S proteins were incubated with the soluble receptor mCEACAM1a[1,4], followed by polyclonal rabbit anti-AVI antibody. The results from the WT were set to 100%, and the experiments were repeated at least three times.

that none of the mutations affected S protein expression and processing. We then investigated if any of the mutations had any effect on the transport of the S protein to the cell surface. HEK293T cells transiently expressing either WT or mutant MHV S protein were incubated with AO4 antibodies on ice and analyzed by flow cytometry. As shown in Fig. 1D, all mutant S proteins were present on the cell surface at a level similar to the WT.

Since all residues that we mutated directly contact the receptor in the NTD/mCEACAM1a complex structure, we then investigated whether or not any of the mutations might affect receptor binding. HEK293T cells transiently expressing either WT or mutant S proteins were incubated with the soluble receptor mCEACAM1a[1,4] on ice, and their receptor binding affinity was measured by flow cytometry. Replacement of either R20 or I22 with alanine significantly decreased S protein binding to the

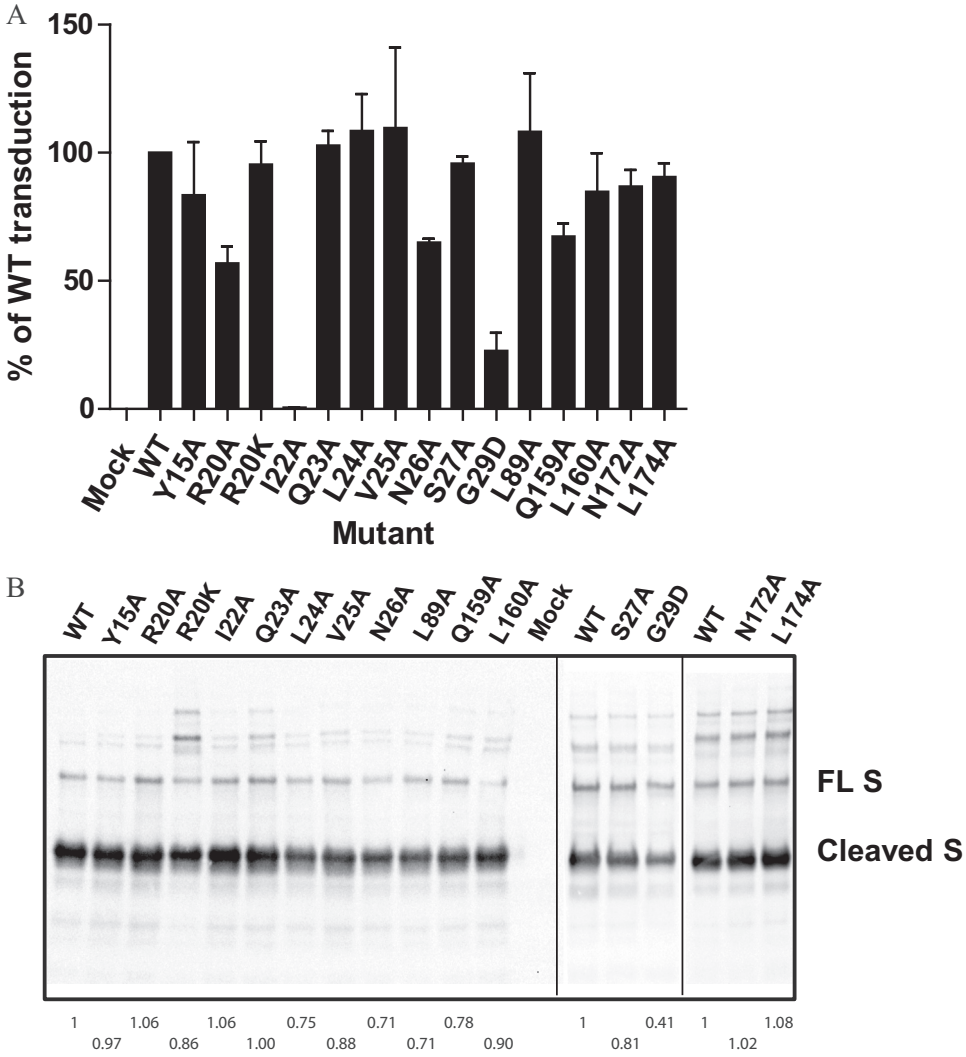

FIG 2 Receptor-dependent entry of lentivirus pseudovirions with WT or mutant S proteins of MHV-A59 on 293/mCEACAM1a cells. (A) Pseudovirus entry was quantitated by luciferase activity at 36 h postinoculation. The results from the WT were set to 100%. The experiments were repeated at least three times, and averages from three experiments with standard deviations are shown. (B) Western blot analysis of WT or mutant S proteins incorporated into pseudovirions. S proteins were detected using goat anti-MHV S antibody AO4. At the bottom are the relative quantification results using Image Lab (Bio-Rad). The experiments were repeated at least three times.

receptor, and their affinities for mCEACAM1a were reduced by 61% and 83% (Fig. 1E), respectively, indicating that both R20 and I22 are critical for receptor binding. None of the other mutants showed a >50% reduction in receptor binding. Replacement of either N26 or N172 with alanine modestly decreased receptor binding by approximate 40% (Fig. 1E). In the NTD/mCEACAM1a structure, three residues, Y15, L89, and L160, in the NTD make direct contact with the critical residue I41 in the receptor. Surprisingly, the introduction of an alanine mutation into either the Y15, L89, or L160 position had almost no effect on receptor binding.

To investigate whether any of the mutations influenced S protein-mediated virus entry, HEK293 cells stably expressing mCEACAM1a (293/mCEACAM1a cells) were transduced with MHV S protein-pseudotyped lentiviruses, and their infectivity was measured according to luciferase activities. As shown in Fig. 2, replacement of I22 with alanine had no effect on S protein incorporation into pseudovirions but reduced S protein-mediated virus entry by more than 99%, indicating that I22 is essential for virus entry, in agreement with our previous report (24). The R20A, N26A, and Q159A mutants also had WT levels of S proteins in pseudovirions but markedly reduced virus entry,

suggesting that R20, N26, and Q159 are also important for virus entry. The G29D substitution reduced S protein incorporation into pseudovirions, likely contributing to its reduction in virus entry. All of other mutants, including Y15A, L89A, and L160A, gave virus entry and S protein incorporation into pseudovirions at levels similar to those of the WT (Fig. 2B).

I41 in mCEACAM1a is located in the middle of the essential CC′ loop and has been proposed to be an essential residue for receptor activity (25). In the NTD/mCEACAM1a complex structure, I41 of the receptor makes contact with Y15, L89, and L160 of the S protein, as part of the first hydrophobic patch interactions. However, as shown in Fig. 2B and Fig. 3A, none of the Y15A, L89A, and L160A mutants showed any significant reductions of binding to the receptor and virus entry, raising questions about their role in receptor binding and virus entry. Since a hydrophobic interaction tends to have redundancy, we then investigated whether double or triple mutations in these positions of the S protein influenced receptor binding and virus entry. All of the double or triple mutants as well as the wild type were expressed and incorporated into pseudotype virions efficiently (Fig. 3B). While Y15A/L89A and L89/L160A bound to the receptor at levels similar to those of the WT S protein, Y15A/L160A greatly reduced receptor binding by over 65% (Fig. 3A), compared to the WT, indicating that interactions between I41 of the receptor and Y15 and L160 of the S protein are important for virus binding. Surprisingly, the Y15A/L160A double mutant entered 293/mCEACAM1a cells as efficiently as the WT (Fig. 3A). As a recent study on virus entry mediated by the Middle East respiratory syndrome CoV (MERS-CoV) S protein revealed that the abundance of the receptor on the cell surface might influence the outcomes of virus entry and receptor binding (26), we reasoned that the presence of high levels of receptors on the 293/mCEACAM1a surface might cause the discrepancy between receptor binding and virus entry. Mouse 17Cl.1 cells are commonly used to grow MHVs and have a relatively lower level of mCEACAM1a on the cell surface than our 293/mCEACAM1a cells (data not shown). We then evaluated virus entry of the Y15A/L160A double mutant in 17Cl.1 cells. As shown in Fig. 3C, the Y15A/L160A mutant S protein mediated virus entry at only about 10% of the WT level.

We previously showed that the S protein of MHV-A59 mediated the formation of receptor-independent syncytia (RIS) in HEK293T cells upon high-pH, such as pH 8.0 but not pH 6.5, triggering (27–29). As shown in Fig. 4A, while treatment of HEK293T cells transiently expressing the WT S protein at pH 6.5 induced levels only slightly above the background level of RIS, large RIS were formed when WT S-expressing cells were incubated at pH 8.0, in agreement with our previous report (27). Surprisingly, G29D showed extensive formation of RIS even at pH 6.5 (Fig. 4A). A significant amount of the S1 subunit was also detected in the supernatant of cells expressing the G29D mutant (Fig. 4B), indicating that the replacement of G29 with aspartic acid triggered spontaneous conformational changes of S proteins and caused the displacement of S1 subunits from S proteins.

To parse out the roles of G29 in conformational changes of the S protein, we further mutated G29 to A, K, M, F, P, and T. None of these mutations had a significant effect on MHV S protein expression, processing, and transportation to the cell surface of HEK293T cells (Fig. 5A and B). Next, we determined if any mutations affected soluble receptor binding to the S protein. HEK293T cells transiently expressing mutant S proteins were incubated with the soluble receptor and analyzed by flow cytometry. Although all G29 mutants showed WT levels of receptor binding regarding the percentage of positive cells (Fig. 5C), the mean fluorescence intensity (MFI) of positive cells for all G29 mutants, except for G29P, was lower than that of the WT (Fig. 5D), especially for G29D and G29T. The lower MFI likely resulted from different amounts of S1 shedding from HEK293T cells among different G29 mutants (Fig. 5A, bottom). Since S1 shedding tends to correlate with RIS formation, we then determined if any mutation affected high-pH-triggered RIS. All mutant S proteins except for the G29P mutant had a significant enhancement of high-pH-triggered RIS (Fig. 6), showing a strong correlation with the S1 shedding results. Among all G29 mutants, G29D and G29T shed the largest amount of S1 into the

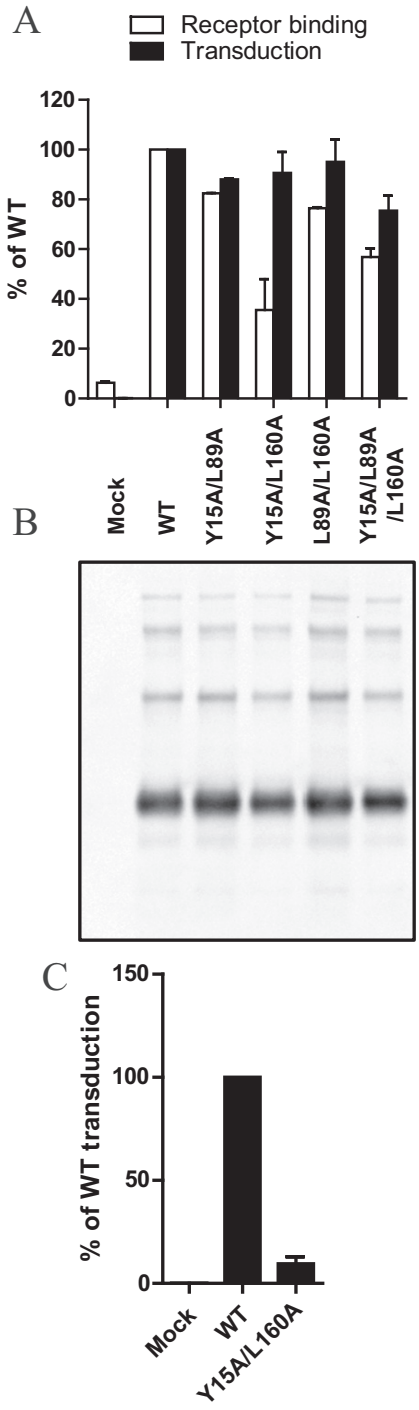

FIG 3 Analysis of receptor binding and receptor-dependent entry of I41-interacting mutant S proteins. (A) Receptor binding and transduction on 293/mCEACAM1a cells by pseudovirions with mutant S proteins. The results from the WT were set as 100%. The experiments were repeated at least three times, and averages from three experiments with standard deviations are shown. (B) Western blot analysis of WT or mutant S proteins incorporated into pseudovirions. The experiments were repeated at least three times. (C) Receptor-dependent entry of pseudovirions into 17Cl.1 cells. The experiments were repeated at least three times, and averages from three experiments with standard deviations are shown.

medium and gave pH-independent RIS. In contrast, G29P shed a minimal amount of S1 and gave only a background level of RIS, even at pH 8.0, indicating that the G29P substitution might introduce structural restraints and prevent the conformational changes of the S protein triggered by high pH.

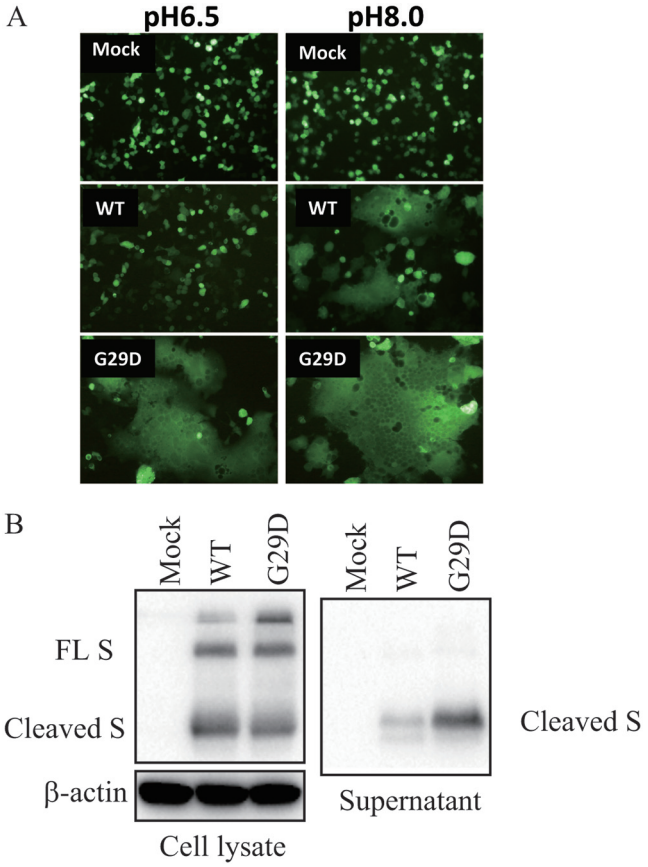

FIG 4 Receptor-independent syncytia mediated by the WT or G29D mutant MHV-A59 S protein. (A) pH 8.0-triggered RIS on HEK293T cells. HEK293T cells transiently coexpressing eGFP with either the WT or G29D mutant MHV S protein were incubated in medium at either pH 6.5 or 8.0 for 6 h. Representative pictures are shown. (B) Western blot analysis of S1 protein shedding into the supernatant. HEK293T cells were transfected with plasmids encoding either the WT or G29D mutant MHV S protein. Cells were fed with fresh serum-free SMM-293-T1 medium. After another 24-h incubation, the supernatant was harvested, concentrated (40-fold), and analyzed by Western blotting with goat anti-MHV S antibody AO4.

To determine whether or not any G29 mutation affects virus entry, we transduced 293/mCEACAM1a cells with either WT or G29 mutant S protein-pseudotyped lentiviruses. All G29 mutants showed a significant reduction in virus entry to different extents (Fig. 7A). However, G29D, G29F, G29K, G29M, and G29T had significantly smaller amounts of S proteins in pseudovirions (Fig. 7B) than the WT, which might partially contribute to the reduction in virus entry. G29A also showed slightly less S protein incorporation into pseudovirions. Interestingly, although G29P had almost WT levels of S protein incorporation in pseudovirions (Fig. 7B), their transduction efficiencies were significantly decreased. The G29P mutation reduced transduction by more than 85%, supporting the notion that the G29P mutation might hinder the conformational changes of S proteins triggered by receptor binding. To further evaluate whether G29P had any defect in conformational changes triggered by receptor binding, we performed limited trypsin digestion analysis on S proteins. Purified pseudovirions with MHV S proteins were incubated with the soluble receptor at 37°C and treated with limited trypsin digestion on ice. Consistent with our previous report (27), upon limited trypsin digestion, several new bands were generated in WT S proteins triggered by receptor binding at 37°C, including a new ~60-kDa band without boiling and dithiothreitol (DTT) treatment (Fig. 7C, left, lane 3) and several bands (25 kDa, 65 kDa, and 120 kDa, etc.) in the boiled and DTT-treated sample (Fig. 7C, right, lane 3), when detected with polyclonal goat anti-MHV S AO4 antibody. In contrast, there was no significant change in the overall pattern of G29P mutant S proteins (Fig. 7C, left, lane 6, and right, lane 6)

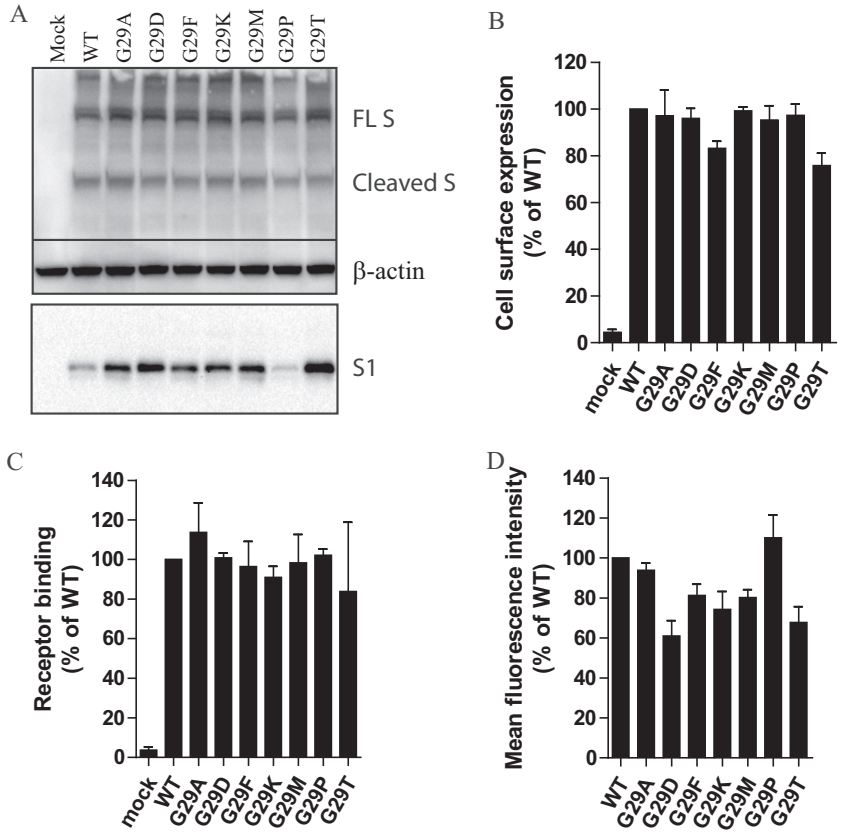

FIG 5 Analysis of expression and receptor binding of G29 mutant S proteins of MHV-A59 on HEK293T cells. (A) Western blot analysis of expression of G29 mutant MHV-A59 S proteins on HEK293T cells. (Top) S protein expression in cell lysates detected using goat anti-MHV S antibody AO4; (middle) β-actin; (bottom) Western blot analysis of S1 shedding in the supernatant. The supernatant was concentrated 40-fold. FL S, full-length S protein. The experiments were repeated at least three times. (B) Analysis of surface expression of G29 mutant MHV-A59 S proteins by flow cytometry. HEK293T cells transiently expressing either WT or mutant S proteins were stained with polyclonal goat anti-MHV S antibody AO4. The amount of WT S protein on the cell surface was set to 100%. The experiments were repeated at least three times, and averages from three experiments with standard deviations are shown. (C) Analysis of receptor binding activities of WT and G29 mutant S proteins by flow cytometry. HEK293T cells transiently expressing either WT or G29 mutant MHV S proteins were incubated with the soluble receptor mCEACAM1a[1,4], followed by polyclonal rabbit anti-AVI antibody. The results from the wild type were set to 100%, the experiments were repeated at least three times, and averages from three experiments with standard deviations are shown. (D) Mean fluorescence intensity from panel C.

upon receptor binding and limited trypsin digestion, compared to the controls, indicating that there was a lack of major conformational changes in G29P mutant S proteins when triggered by receptor binding.

In the NTD structure, G29 is located close to the end of the β1-sheet and at the center of a turn (Fig. 8A). Interestingly, G29 is conserved among only some MHV strains, including MHV-A59, MHV-JHM, MHV-1, and MHV-4 but not in MHV-2 and MHV-3 (Fig. 8B). In MHV-2 and -3, residues at positions 28 and 30 of the S protein also differ from those in other MHV strains but are conserved between them (Fig. 8B). In the NTD structure, the side chains of N28 and A30 are very close, about 3.4 Å apart (Fig. 8A). We hypothesized that D28 and S30 of the MHV-2 and MHV-3 S proteins might form hydrogen bonds between them to stabilize the structural turn required for the S proteins of MHV-2 and MHV-3. We then constructed two mutants in the background of the S protein of MHV-A59 with the corresponding residues 28 to 30 of the S protein of MHV-2, the N28D/G29T double mutant and the N28D/G29T/A30S triple mutant. We reasoned that the N28D/G29T/A30S triple mutant might be more stable than the N28D/G29T double mutant because of potential

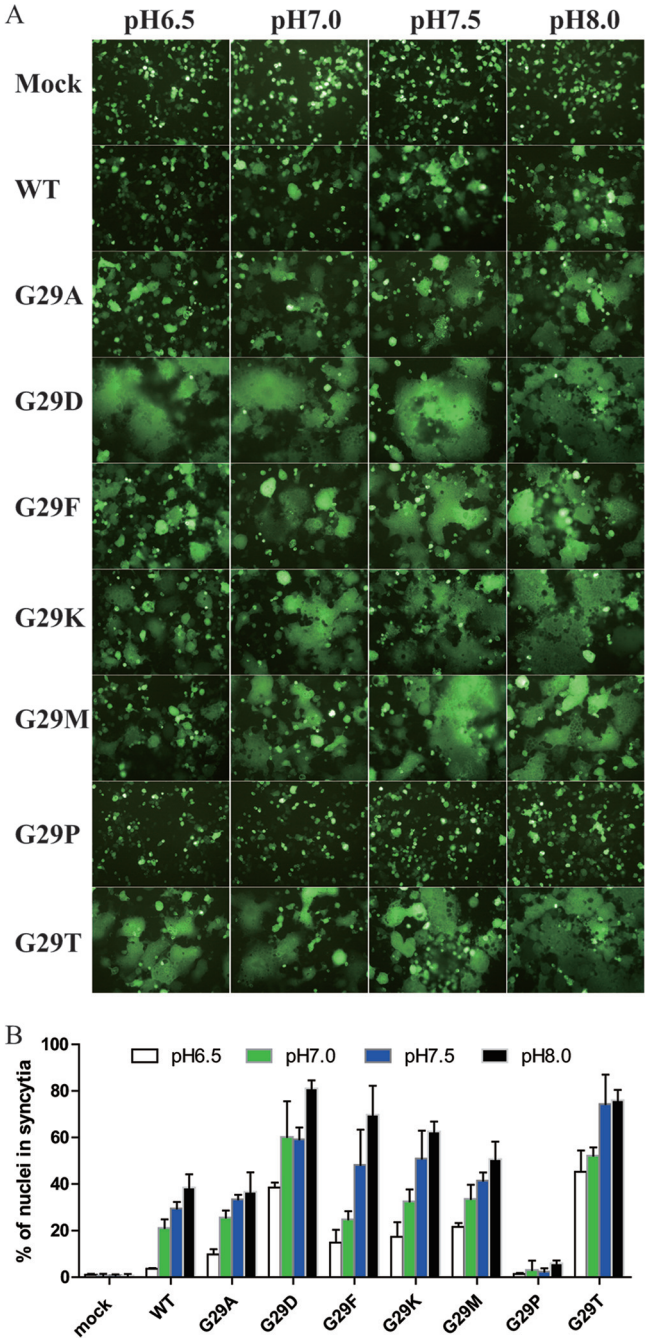

FIG 6 Elevated pH-induced receptor-independent syncytium formation in HEK293T cells by G29 mutant S proteins. (A) HEK293T cells transiently expressing WT or G29 mutant MHV-A59 S proteins with eGFP were incubated at the indicated pHs for 6 h. Representative pictures are shown. (B) Quantitative analysis of syncytia in panel A. The experiments were repeated three times, and data from one representative experiment are shown.

extra hydrogen bonding between N28D and A30S. As shown in Fig. 8, theN28D/G29T/A30S triple mutant was expressed at a level similar to that of the WT S protein (Fig. 8C), shed amounts of S1 into the supernatant similar to those shed by the WT (Fig. 8D), and induced slightly more RIS at pH 6.5 and 8.0 (Fig. 8E). In contrast, the N28D/G29T double mutant shed significantly more S1 into the supernatant and induced markedly higher levels of RIS at both pH 6.5 and 8.0 (Fig. 8D and E), consistent with the idea that the absence of hydrogen bonding between D28 and

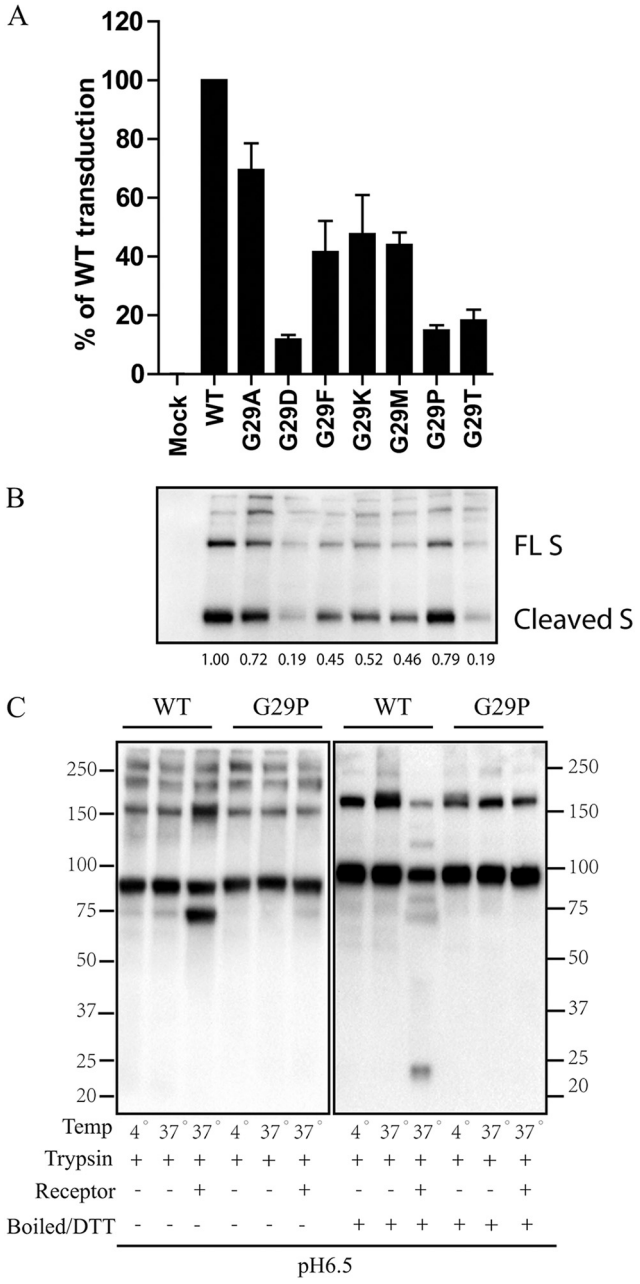

FIG 7 Receptor-dependent entry of lentivirus pseudovirions with G29 mutant S proteins of MHV-A59 in 293/mCEACAM1a cells and limited trypsin digestion analysis of conformational changes of G29P mutant S proteins upon receptor binding. (A) Pseudovirus entry was quantitated by luciferase activity at 36 h postinoculation. The results from the WT were set to 100%. The experiments were repeated at least three times, and averages from three experiments with standard deviations are shown. (B) Western blot analysis of WT or G29 mutant S proteins incorporated into pseudovirions. S proteins were detected using goat anti-MHV S antibody AO4. At the bottom are the relative quantification results using Image Lab (Bio-Rad). The experiments were repeated at least three times. (C) Limited trypsin digestion of WT or G29P mutant S proteins of MHV-A59. Purified pseudovirions with WT or G29P mutant S proteins were incubated with the soluble receptor on ice for 30 min, shifted to 37°C for 30 min, and then digested on ice with 20 μg/ml trypsin for 20 min. S proteins and fragments were detected using goat anti-MHV S antibody AO4. (Left) Without boiling and with no DTT; (right) with boiling and DTT. The experiments were repeated three times, and data from one representative experiment are shown.

A30 in the N28D/G29T double mutant might destabilize the S protein. The N28D/G29T/A30S triple mutant S proteins were incorporated into pseudovirions slightly less than the WT (Fig. 8F) and mediated virus entry at a level similar to that of the WT (Fig. 8G).

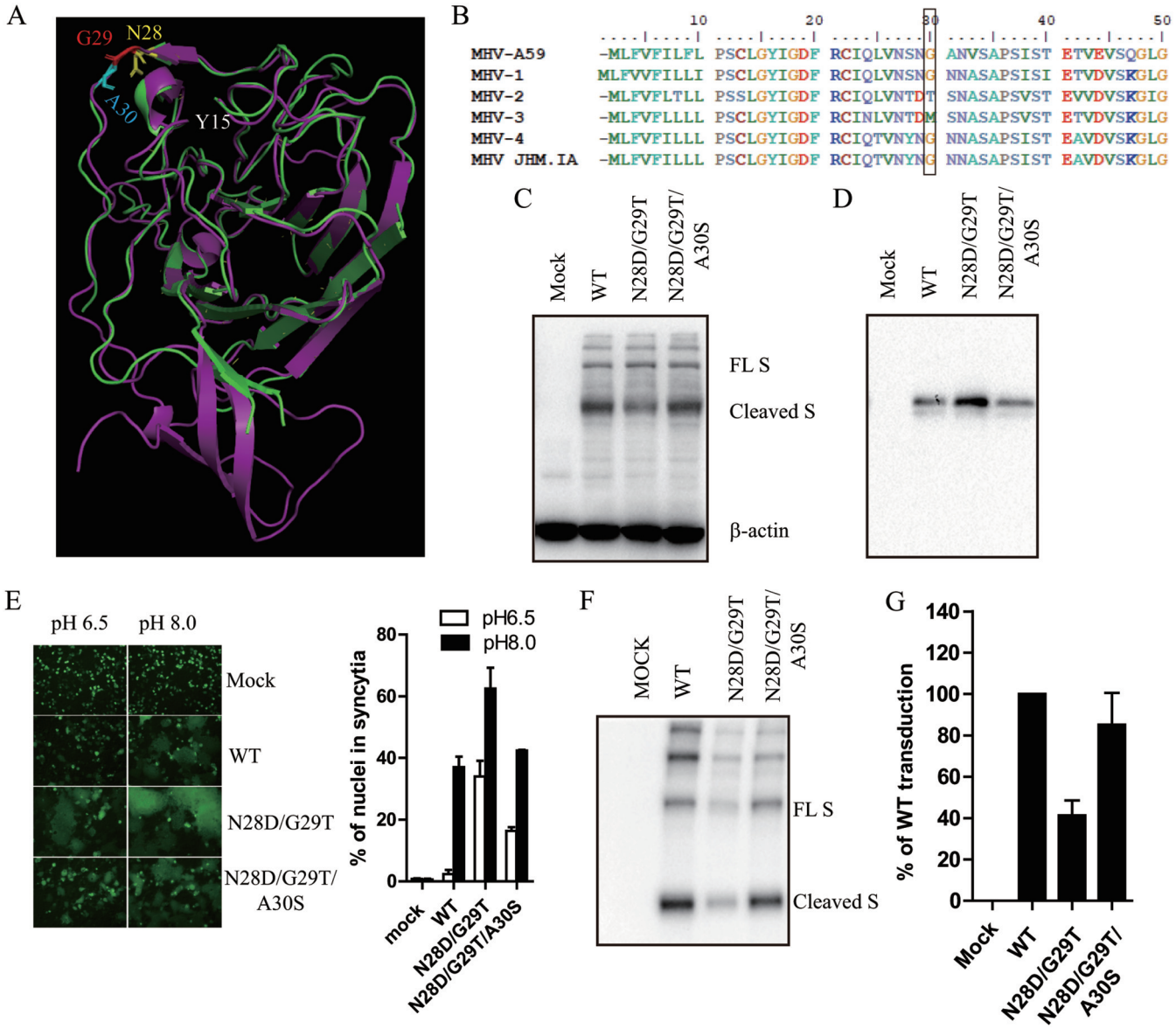

FIG 8 Systemic analysis of N28D/G29T double mutant and N28D/G29T/A30S triple mutant MHV-A59 S proteins. (A) Cartoon representation of the alignment of the crystal structure of the NTD in the NTD/mCEACAM1a complex (green) (PDB accession number 3R4D) with the cryo-electron microscopy (EM) structure of the NTD in the native trimeric S protein of MHV-A59 (purple) (PDB accession number 3JCL). N28 (yellow), G29 (red), and A30 (cyan) are shown as sticks. (B) Amino acid sequence alignment of S proteins of different MHV strains. (C) Western blot analysis of expression of N28D/G29T double mutant and N28D/G29T/A30S triple mutant MHV-A59 S proteins on HEK293T cells. MHV S proteins were detected using goat anti-MHV S antibody AO4. (D) S1 shedding. The 40-fold-concentrated supernatant was separated in a 4 to 20% SDS-PAGE gel and blotted with goat anti-MHV S antibody AO4.The experiments were repeated at least three times. (E) Receptor-independent syncytia mediated by double or triple mutant MHV-A59 S proteins. (Left) Representative images of RIS; (right) quantitative analysis of RIS in the left panel. (F) Western blot analysis of mutant S protein incorporation into pseudovirions. (G) Receptor-dependent virus entry. The results for the WT are set to 100%, the experiments were repeated at least three times, and averages from three experiments with standard deviations are shown.

We previously found that the Y320A mutant also induced pH-independent RIS (21). Y320 is located in the SD-1 subdomain of the CTD and interacts with the core subdomain of the S1 subunit of the CTD (Fig. 9A). We then investigated whether stabilization of the NTD by a G29P mutation had any effect on Y320A mutation-triggered pH- and receptor-independent syncytium formation. As shown in Fig. 9B and C, the G29P substitution had almost no effect on pH- and receptor-independent syncytium formation triggered by the Y320A mutation, suggesting that stabilizing the NTD has almost no effect on conformational changes of the S protein originating from the CTD.

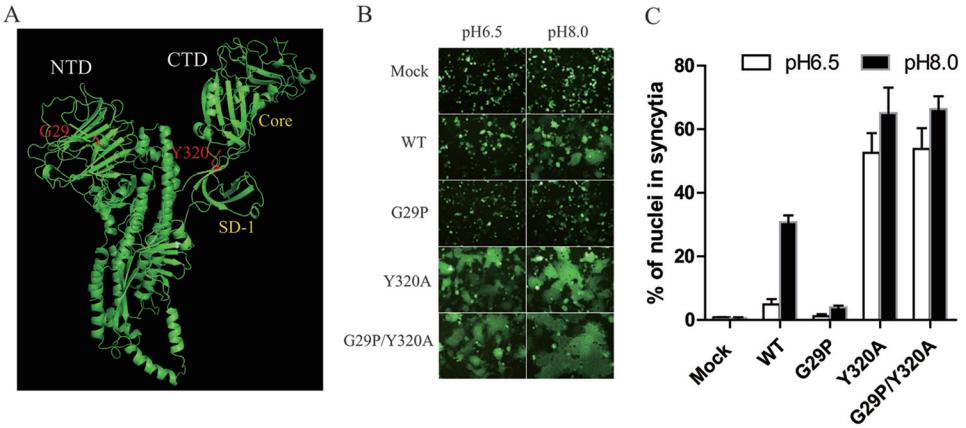

FIG 9 Effect of the G29P mutation on pH-independent RIS triggered by the Y320 mutation. (A) Cartoon representation of the cryo-EM structure of a single monomer of the trimeric S protein of MHV-A59 (PDB accession number 3JCL). G29 and Y320 are shown in red. (B) Receptor-independent syncytia mediated by mutant MHV-A59 S proteins. HEK293T cells transiently expressing eGFP and either WT or mutant S proteins were incubated in medium at either pH 6.5 or 8.0 for 6 h. Representative images are shown. (C) Quantitative analysis of data in panel A. Data shown are representative of results from three independent experiments.

DISCUSSION

It is well established that native trimeric S protein exists in a metastable state prior to interaction with the receptor and that receptor binding causes conformational changes of the S protein and leads to the dissociation of S1 from the S protein, the formation of a six-helix bundle, and fusion of the viral and cellular membranes. Recently, series of structures of S proteins of various coronaviruses from multiple genera in different conformational states, such as those without receptor binding (30–35), those with a receptor complex (18, 24, 36–39), and those in a postfusion conformation (40, 41), have been reported. Surprisingly, structural alignment between the native trimeric MHV S protein and the MHV NTD/mCEACAM1a complex reveals that there is an absence of major conformational changes in the MHV NTD upon receptor binding (Fig. 8A). It is worth noting that receptor binding-induced conformational changes in the MHV NTD might be too transient to be captured by structure studies, or the MHV NTD/mCEACAM1a complex could not go through any conformational changes, simply because complex crystallization was performed at 4°C and not at 37°C.

Does binding to mCEACAM1a trigger any conformational change in the MHV NTD? If so, how? There are 14 residues in the MHV NTD interacting with mCEACAM1a, and most of them are located on the N terminus of the MHV S protein and form a loop and a β1-sheet (24). Among them, I22 is essential for receptor binding and virus entry, in agreement with our previous report (24). Unexpectedly, we found that G29 might play important roles in conformational changes of the S protein triggered by either receptor binding or high pH. G29 is located on the top of the trimeric S protein, close to the end of the β1-sheet, and at the center of a turn (Fig. 8A). Replacement of G29 with either aspartic acid or threonine might alter the local conformation in the NTD by extending the β1-sheet and disrupting the turn and may lead to conformational changes of the NTD, resulting in the spontaneous dissociation of S1 subunits from the S protein and the formation of pH- and receptor-independent syncytia. G29A, G29F, G29K, and G29M mutations might also change the local conformation to lower degrees and showed a significant enhancement of high-pH-triggered RIS (Fig. 6). In contrast, the G29P substitution had no effect on S protein processing, receptor binding, and S protein incorporation into pseudovirions (Fig. 5 and 7), suggesting that its overall conformation prior to receptor binding is very similar to that of the WT S protein. Glycine and proline are two residues that are often found in β-turns. However, while glycine has no side chain and is the most sterically flexible residue, proline has the cyclic side chain and is the most conformationally restricted amino acid residue. We reason that the inherent

rigid property of proline to maintain the turn in the G29P mutant might hinder the conformational change of the S protein from receptor binding, resulting in a >85% reduction in the transduction efficiency. This notion was further supported by our limited trypsin digestion results, where binding of the G29P S protein to the soluble receptor induced only minimal conformational changes of the S protein (Fig. 7C). Since G29 is also at the NTD/mCEACAM1a interaction interface, we propose that G29 might be one of the residues critical for the early initiation of receptor binding-induced conformational changes of the S protein in the MHV-A59 strain. The G29P mutant also showed a significant defect in high-pH-triggered receptor-independent syncytium formation, indicating that the proline substitution likely stabilizes the overall conformation of the S protein.

Interestingly, G29 and its surrounding residues are not well conserved among different strains of MHV (Fig. 8B); S proteins of MHV-2 and MHV-3 have D at position 28, T or M at position 29, and S at position 30. D28 and S30 in MHV-2 and MHV-3 likely form hydrogen bonds to facilitate structural turn formation around residue 29 to stabilize the prefusion conformation of the MHV S protein. Disrupting this interaction results in the spontaneous dissociation of the S1 subunit from the S protein and pH-independent RIS. These results led us to conclude that the exact residue at position 29 might not be important, but the structural turn and its flexibility might be essential instead.

In the cocrystal structure of the MHV S NTD/mCEACAM1a complex, there are two hydrophobic patches essential for the interaction of the NTD and mCEACAM1a (24). The first hydrophobic patch includes interactions of I41 of mCEACAM1a with Y15, L89, and L160 of MHV S, while the second hydrophobic patch is composed of interactions of V49, M54, and F56 of mCEACAM1a with I22 and Y162 of the MHV NTD. I41 of mCEACAM1a is essential for virus entry (25). Surprisingly, mutating all three I41-interacting residues, Y15, L89, and L160, to alanine reduced the binding of the S protein to mCEACAM1a by only 43% and had almost no effect on S-mediated virus entry, consistent with the idea that hydrophobic interactions tend to have redundancy. The difference observed between binding affinity and virus entry likely results from the inherent difference between the two assays. The virus binding assay was performed at 4°C for 1 h, at which membrane fusion could not occur, whereas the virus entry assay was done at 37°C overnight, at which membrane fusion could occur. Since membrane fusion is irreversible, it might drive weak binding for successful virus entry when large amounts of receptors are present and when it is given enough time. Similar phenomena have been observed for other coronaviruses (17, 26, 42) and other enveloped viruses (43, 44). In the second hydrophobic patch, I22 of the NTD seems to be essential. The replacement of I22 with alanine dramatically decreased virus binding (Fig. 1) and almost abolished virus entry (Fig. 2). There are two residues in mCEACAM1a interacting with I22 of the S protein, M54 and F56, where replacement of M54 with lysine or F56 with threonine in mCEACAM1a significantly decreased virus entry (7), indicating that interactions between I22 of the S protein and M54 and F56 of mCEACAM1a are critical for virus entry. I22 of the NTD and I41 of mCEACAM1a are like two hydrophobic anchors. They do not interact with each other, but they anchor the interaction between the S protein and mCEACAM1a. Removal of either "anchor" is detrimental to receptor binding and virus entry, but modification of the "anchoring place" is less influential on viral infection.

S proteins of all CoVs contain both an NTD and a CTD, but different CoVs evolve to use either the NTD or CTD to bind their cognate receptor. Some CoVs, such as MERS-CoV, use their CTDs to bind protein receptors and NTDs to bind sugar moieties (45, 46). One intriguing question is whether there is any cross-domain communication between the NTD and CTD during conformational changes of the S protein leading to virus entry. The G29P mutation stabilizes the MHV-A59 S protein (Fig. 5A) and hinders the conformational changes of the S protein initiated from the NTD (Fig. 7) but has almost no effect on pH- and receptor-independent syncytium formation initiated by a CTD mutation, Y320A, indicating that there might be minimal cross-domain communication between the NTD and CTD during conformational changes of the S protein, at least in MHV-A59.

In summary, we determined the biological contribution of individual receptor-contacting residues to receptor binding and virus entry and found that I22 of the NTD is one of the anchors for receptor binding and virus entry. Surprisingly, we also identified that a structural turn immediately following the β1-sheet and its flexibility are critical for conformational changes of the MHV S protein triggered by either receptor binding or high pH.

MATERIALS AND METHODS

Cell culture. HEK293 cells, HEK293T cells, HEK293T cells stably expressing mCEACAM1a (293/mCEACAM1a), and 17Cl.1 cells were maintained in Dulbecco's modified Eagle's medium (DMEM) (Invitrogen, Carlsbad, CA) supplemented with 10% fetal bovine serum (FBS) and 2% penicillin-streptomycin-amphotericin B (Fungizone) (Invitrogen) at 37°C with 5% CO_2.

Construction of MHV S mutants. DNA encoding the codon-optimized full-length MHV-A59 S protein (GenBank accession number P11224.2) was synthesized (GenScript, Piscataway, NJ, USA) and cloned between the BamHI and NotI sites of pcDNA3.1 to generate the pcDNA3-MHV S construct (12). All mutagenesis was carried out using a Q5 mutagenesis kit (NEB, MA, USA). After the entire coding sequences were verified by sequencing, the BamHI- and NotI-containing mutated S gene was cloned back into pcDNA3-MHV S.

Analysis of MHV S protein expression on the cell surface. HEK293T cells were transfected with 2 μg of plasmids encoding either the wild-type or mutant S protein using polyethyleneimine (PEI) (Polysciences Inc.). Forty hours later, cells were detached from the plate by incubating them with phosphate-buffered saline (PBS) with 1 mM EDTA for 5 min at 37°C. After washing twice with PBS plus 2% normal donkey serum (NDS), cells were incubated with polyclonal goat anti-MHV S protein antibody AO4 at a dilution of 1:100 for 1 h on ice, followed by staining with phycoerythrin (PE)-conjugated donkey anti-goat IgG (1:100 dilution; Jackson Immunoresearch) for 1 h on ice. After washing three times with PBS plus 2% NDS, cells were fixed with 1% paraformaldehyde in PBS and analyzed by flow cytometry.

Binding of soluble murine receptor. Human HEK293T cells transiently expressing either wild-type or mutant S proteins were lifted with PBS plus 1 mM EDTA. After washing twice with PBS plus 2% NDS, cells (about 2×10^5) were incubated with 10 μg of soluble mCEACAM1a[1,4] for 1 h on ice, followed by rabbit polyclonal anti-AVI tag antibody (1:200 dilution) (Shanghai Enzyme-Linked Biotechnology Co., Shanghai, China). Cells were further stained with Alexa Fluor 488-conjugated goat anti-rabbit IgG (1:200), fixed with 1% paraformaldehyde, and analyzed by flow cytometry.

Production of MHV S-pseudotyped lentivirus and transduction of pseudovirions. MHV S protein-pseudotyped viruses were produced as described previously (27), with minor modifications. Briefly, a plasmid encoding either the wild-type or mutant S protein was cotransfected into HEK293T cells with pLenti-Luc-GFP (a gift from Fang Li, Duke University) and psPAX2 (Addgene, Cambridge, MA) at a molar ratio of 1:1:1 using PEI. The next day, cells were fed with fresh medium at pH 6.5. After another 24-h incubation, the virus supernatant was harvested and filtered through a 0.45-μm filter. To quantify MHV-A59 S protein-mediated entry of pseudovirions, 293/mCEACAM1a cells were seeded at 25% confluence in a 12-well plate. The next day, cells were inoculated with 500 μl of 1:1-diluted viruses, which were normalized based on a p24 enzyme-linked immunosorbent assay (ELISA) (Beijing Key-Bio Biotech, Beijing, China). After a 40-h incubation at 37°C, cells were lysed at room temperature with 120 μl of medium with an equal volume of Steady-glo (Promega, Madison, WI, USA). The transduction efficiency was determined by quantitation of luciferase activity using a Modulus II microplate reader (Turner Biosystem, Sunnyvale, CA). All experiments were repeated at least three times.

Detection of viral spike glycoproteins by Western blotting. To evaluate S protein expression in cells, HEK293T cells were transfected with 2 μg of plasmids encoding either the wild-type or mutant S protein using PEI. Forty hours later, cells were lysed by using cell lysis buffer (50 mM Tris HCl [pH 7.4], 150 mM NaCl, 2 mM EDTA, 1% Triton X-100, 0.1% SDS, 1$\times$ protease inhibitor cocktail [Roche]). After a 30-min incubation on ice, the cell lysate was centrifuged at 10,000 $\times$ *g* for 10 min at 4°C to remove nuclei, and the supernatant was collected. To determine S protein incorporation into pseudovirions, the virion-containing supernatant, which was normalized based on p24 ELISA results, was pelleted through a 20% sucrose cushion at 30,000 rpm at 4°C for 2 h in a Beckman SW41 rotor (43). Viral pellets were resuspended in PBS. The cell lysate and pseudovirion pellet were separated on a 4 to 15% SDS-PAGE gel and transferred to a nitrocellulose blot. The MHV S protein was detected using polyclonal goat anti-MHV S protein antibodies (AO4) (1:2,000), and the blot was further stained with horseradish peroxidase-conjugated rabbit anti-goat IgG (1:10,000) and then visualized with the Clarity Western ECL substrate (Bio-Rad, Hercules, CA, USA).

High-pH-triggered and receptor-independent cell-cell fusion assays. High-pH-triggered and receptor-independent cell-cell fusion assays were described previously (27). Briefly, human HEK293T cells were cotransfected with plasmids encoding the WT or mutant MHV-A59 S glycoprotein and green fluorescent protein (GFP) using PEI. Twenty-four hours later, cells were fed with fresh medium at the indicated pHs. After a 6-h incubation, cells were fixed with 4% paraformaldehyde in PBS, and images (enhanced GFP [eGFP] and phase) of syncytia were captured with a Nikon TE2000 epifluorescence microscope running MetaMorph software (Molecular Devices). All experiments were done in triplicates and repeated at least three times. For each mutant, three randomly selected images were chosen, and for each image, the total number of nuclei in syncytia and the total number of cells were counted and the percentage of nuclei in syncytia was calculated as the total number of nuclei in syncytia/number of total cells $\times$ 100.

Analysis of conformational changes of S proteins on pseudovirions by limited trypsin digestion. Analysis of S protein conformation changes using limited trypsin digestion was performed as described previously, with minor modifications (27). Briefly, purified MHV S protein-pseudotyped virions were incubated with or without 10 μg of soluble mCEACAM1a[1,4] for 30 min on ice to allow receptor binding and then shifted to either 4°C or 37°C for 30 min. After incubation, the virus-receptor mixture was quickly cooled to 4°C. Tosylsulfonyl phenylalanyl chloromethyl ketone (TPCK)-treated trypsin was then added to each well to a final concentration of 20 μg/ml. After a 30-min incubation, a 5-fold excess of a soybean trypsin inhibitor was added. Half of the samples were boiled with DTT and then separated on a 4 to 15% SDS-PAGE gel, and the other half, without DTT and boiling, were directly separated on a 4 to 15% SDS-PAGE gel. After transfer of the samples to a nitrocellulose blot, MHV-A59 S proteins were detected with polyclonal goat anti-MHV S antibody AO4 (1:2,000).

ACKNOWLEDGMENTS

This work was supported by grants from the National Natural Science Foundation of China (31670164, 31970171, and 81702013), the National Science and Technology Major Project (2018ZX10101-001), the CAMS Innovation Fund for Medical Sciences (2016-12M-1-014), and the CAMS general fund (2016ZX310052).

REFERENCES

1. Masters PS, Perlman S. 2013. Coronaviridae, p 825–858. *In* Knipe DM, Howley PM, Cohen JI, Griffin DE, Lamb RA, Martin MA, Racaniello VR, Roizman B (ed), Fields virology, 6th ed, vol 1. Lippincott Williams & Wilkins, Philadelphia, PA.
2. King AMQ, Adams MJ, Carstens EB, Lefkowitz EJ (ed). 2012. Virus taxonomy. Classification and nomenclature of viruses. Ninth report of the International Committee on Taxonomy of Viruses. Elsevier Academic Press, San Diego, CA.
3. Dveksler GS, Pensiero MN, Cardellichio CB, Williams RK, Jiang GS, Holmes KV, Dieffenbach CW. 1991. Cloning of the mouse hepatitis virus (MHV) receptor: expression in human and hamster cell lines confers susceptibility to MHV. J Virol 65:6881–6891.
4. Williams RK, Jiang GS, Holmes KV. 1991. Receptor for mouse hepatitis virus is a member of the carcinoembryonic antigen family of glycoproteins. Proc Natl Acad Sci U S A 88:5533–5536. https://doi.org/10.1073/pnas.88.13.5533.
5. Kuespert K, Pils S, Hauck CR. 2006. CEACAMs: their role in physiology and pathophysiology. Curr Opin Cell Biol 18:565–571. https://doi.org/10.1016/j.ceb.2006.08.008.
6. Williams RK, Jiang GS, Snyder SW, Frana MF, Holmes KV. 1990. Purification of the 110-kilodalton glycoprotein receptor for mouse hepatitis virus (MHV)-A59 from mouse liver and identification of a nonfunctional, homologous protein in MHV-resistant SJL/J mice. J Virol 64:3817–3823.
7. Peng G, Yang Y, Pasquarella JR, Xu L, Qian Z, Holmes KV, Li F. 2017. Structural and molecular evidence suggesting coronavirus-driven evolution of mouse receptor. J Biol Chem 292:2174–2181. https://doi.org/10.1074/jbc.M116.764266.
8. Bosch BJ, Martina BE, Van Der Zee R, Lepault J, Haijema BJ, Versluis C, Heck AJ, De Groot R, Osterhaus AD, Rottier PJ. 2004. Severe acute respiratory syndrome coronavirus (SARS-CoV) infection inhibition using spike protein heptad repeat-derived peptides. Proc Natl Acad Sci U S A 101:8455–8460. https://doi.org/10.1073/pnas.0400576101.
9. Liu S, Xiao G, Chen Y, He Y, Niu J, Escalante CR, Xiong H, Farmar J, Debnath AK, Tien P, Jiang S. 2004. Interaction between heptad repeat 1 and 2 regions in spike protein of SARS-associated coronavirus: implications for virus fusogenic mechanism and identification of fusion inhibitors. Lancet 363:938–947. https://doi.org/10.1016/S0140-6736(04)15788-7.
10. Tripet B, Howard MW, Jobling M, Holmes RK, Holmes KV, Hodges RS. 2004. Structural characterization of the SARS-coronavirus spike S fusion protein core. J Biol Chem 279:20836–20849. https://doi.org/10.1074/jbc.M400759200.
11. Howard MW, Travanty EA, Jeffers SA, Smith MK, Wennier ST, Thackray LB, Holmes KV. 2008. Aromatic amino acids in the juxtamembrane domain of severe acute respiratory syndrome coronavirus spike glycoprotein are important for receptor-dependent virus entry and cell-cell fusion. J Virol 82:2883–2894. https://doi.org/10.1128/JVI.01805-07.
12. Ou X, Zheng W, Shan Y, Mu Z, Dominguez SR, Holmes KV, Qian Z. 2016. Identification of the fusion peptide-containing region in betacoronavirus spike glycoproteins. J Virol 90:5586–5600. https://doi.org/10.1128/JVI.00015-16.
13. Hingley ST, Gombold JL, Lavi E, Weiss SR. 1994. MHV-A59 fusion mutants are attenuated and display altered hepatotropism. Virology 200:1–10. https://doi.org/10.1006/viro.1994.1156.
14. Belouzard S, Chu VC, Whittaker GR. 2009. Activation of the SARS coronavirus spike protein via sequential proteolytic cleavage at two distinct sites. Proc Natl Acad Sci U S A 106:5871–5876. https://doi.org/10.1073/pnas.0809524106.
15. Millet JK, Whittaker GR. 2014. Host cell entry of Middle East respiratory syndrome coronavirus after two-step, furin-mediated activation of the spike protein. Proc Natl Acad Sci U S A 111:15214–15219. https://doi.org/10.1073/pnas.1407087111.
16. Bonavia A, Zelus BD, Wentworth DE, Talbot PJ, Holmes KV. 2003. Identification of a receptor-binding domain of the spike glycoprotein of human coronavirus HCoV-229E. J Virol 77:2530–2538. https://doi.org/10.1128/JVI.77.4.2530-2538.2003.
17. Hofmann H, Simmons G, Rennekamp AJ, Chaipan C, Gramberg T, Heck E, Geier M, Wegele A, Marzi A, Bates P, Pohlmann S. 2006. Highly conserved regions within the spike proteins of human coronaviruses 229E and NL63 determine recognition of their respective cellular receptors. J Virol 80:8639–8652. https://doi.org/10.1128/JVI.00560-06.
18. Li F, Li W, Farzan M, Harrison SC. 2005. Structure of SARS coronavirus spike receptor-binding domain complexed with receptor. Science 309:1864–1868. https://doi.org/10.1126/science.1116480.
19. Tusell SM, Schittone SA, Holmes KV. 2007. Mutational analysis of aminopeptidase N, a receptor for several group 1 coronaviruses, identifies key determinants of viral host range. J Virol 81:1261–1273. https://doi.org/10.1128/JVI.01510-06.
20. Wu K, Li W, Peng G, Li F. 2009. Crystal structure of NL63 respiratory coronavirus receptor-binding domain complexed with its human receptor. Proc Natl Acad Sci U S A 106:19970–19974. https://doi.org/10.1073/pnas.0908837106.
21. Ou X, Guan H, Qin B, Mu Z, Wojdyla JA, Wang M, Dominguez SR, Qian Z, Cui S. 2017. Crystal structure of the receptor binding domain of the spike glycoprotein of human betacoronavirus HKU1. Nat Commun 8:15216. https://doi.org/10.1038/ncomms15216.
22. Qian Z, Ou X, Goes LG, Osborne C, Castano A, Holmes KV, Dominguez SR. 2015. Identification of the receptor-binding domain of the spike glycoprotein of human betacoronavirus HKU1. J Virol 89:8816–8827. https://doi.org/10.1128/JVI.03737-14.
23. Kubo H, Yamada YK, Taguchi F. 1994. Localization of neutralizing epitopes and the receptor-binding site within the amino-terminal 330 amino acids of the murine coronavirus spike protein. J Virol 68:5403–5410.
24. Peng G, Sun D, Rajashankar KR, Qian Z, Holmes KV, Li F. 2011. Crystal structure of mouse coronavirus receptor-binding domain complexed with its murine receptor. Proc Natl Acad Sci U S A 108:10696–10701. https://doi.org/10.1073/pnas.1104306108.
25. Tan K, Zelus BD, Meijers R, Liu JH, Bergelson JM, Duke N, Zhang R, Joachimiak A, Holmes KV, Wang JH. 2002. Crystal structure of murine sCEACAM1a[1,4]: a coronavirus receptor in the CEA family. EMBO J 21:2076–2086. https://doi.org/10.1093/emboj/21.9.2076.
26. Kleine-Weber H, Elzayat MT, Wang L, Graham BS, Muller MA, Drosten C,

Pohlmann S, Hoffmann M. 2019. Mutations in the spike protein of Middle East respiratory syndrome coronavirus transmitted in Korea increase resistance to antibody-mediated neutralization. J Virol 93: e001381-18. https://doi.org/10.1128/JVI.01381-18.
27. Li P, Shan Y, Zheng W, Ou X, Mi D, Mu Z, Holmes KV, Qian Z. 2018. Identification of H209 as essential for pH 8-triggered receptor-independent syncytium formation by S protein of mouse hepatitis virus A59. J Virol 92:e00209-18. https://doi.org/10.1128/JVI.00209-18.
28. Sturman LS, Ricard CS, Holmes KV. 1990. Conformational change of the coronavirus peplomer glycoprotein at pH 8.0 and 37°C correlates with virus aggregation and virus-induced cell fusion. J Virol 64:3042–3050.
29. Zelus BD, Schickli JH, Blau DM, Weiss SR, Holmes KV. 2003. Conformational changes in the spike glycoprotein of murine coronavirus are induced at 37°C either by soluble murine CEACAM1 receptors or by pH 8. J Virol 77:830–840. https://doi.org/10.1128/JVI.77.2.830-840.2003.
30. Walls AC, Tortorici MA, Bosch BJ, Frenz B, Rottier PJ, DiMaio F, Rey FA, Veesler D. 2016. Cryo-electron microscopy structure of a coronavirus spike glycoprotein trimer. Nature 531:114–117. https://doi.org/10.1038/nature16988.
31. Walls AC, Tortorici MA, Frenz B, Snijder J, Li W, Rey FA, DiMaio F, Bosch BJ, Veesler D. 2016. Glycan shield and epitope masking of a coronavirus spike protein observed by cryo-electron microscopy. Nat Struct Mol Biol 23:899–905. https://doi.org/10.1038/nsmb.3293.
32. Shang J, Zheng Y, Yang Y, Liu C, Geng Q, Luo C, Zhang W, Li F. 2018. Cryo-EM structure of infectious bronchitis coronavirus spike protein reveals structural and functional evolution of coronavirus spike proteins. PLoS Pathog 14:e1007009. https://doi.org/10.1371/journal.ppat.1007009.
33. Kirchdoerfer RN, Cottrell CA, Wang N, Pallesen J, Yassine HM, Turner HL, Corbett KS, Graham BS, McLellan JS, Ward AB. 2016. Pre-fusion structure of a human coronavirus spike protein. Nature 531:118–121. https://doi.org/10.1038/nature17200.
34. Gui M, Song W, Zhou H, Xu J, Chen S, Xiang Y, Wang X. 2017. Cryo-electron microscopy structures of the SARS-CoV spike glycoprotein reveal a prerequisite conformational state for receptor binding. Cell Res 27:119–129. https://doi.org/10.1038/cr.2016.152.
35. Yuan Y, Cao D, Zhang Y, Ma J, Qi J, Wang Q, Lu G, Wu Y, Yan J, Shi Y, Zhang X, Gao GF. 2017. Cryo-EM structures of MERS-CoV and SARS-CoV spike glycoproteins reveal the dynamic receptor binding domains. Nat Commun 8:15092. https://doi.org/10.1038/ncomms15092.
36. Song W, Gui M, Wang X, Xiang Y. 2018. Cryo-EM structure of the SARS coronavirus spike glycoprotein in complex with its host cell receptor ACE2. PLoS Pathog 14:e1007236. https://doi.org/10.1371/journal.ppat.1007236.
37. Lu G, Hu Y, Wang Q, Qi J, Gao F, Li Y, Zhang Y, Zhang W, Yuan Y, Bao J, Zhang B, Shi Y, Yan J, Gao GF. 2013. Molecular basis of binding between novel human coronavirus MERS-CoV and its receptor CD26. Nature 500:227–231. https://doi.org/10.1038/nature12328.
38. Wang N, Shi X, Jiang L, Zhang S, Wang D, Tong P, Guo D, Fu L, Cui Y, Liu X, Arledge KC, Chen YH, Zhang L, Wang X. 2013. Structure of MERS-CoV spike receptor-binding domain complexed with human receptor DPP4. Cell Res 23:986–993. https://doi.org/10.1038/cr.2013.92.
39. Kirchdoerfer RN, Wang N, Pallesen J, Wrapp D, Turner HL, Cottrell CA, Corbett KS, Graham BS, McLellan JS, Ward AB. 2018. Stabilized coronavirus spikes are resistant to conformational changes induced by receptor recognition or proteolysis. Sci Rep 8:15701. https://doi.org/10.1038/s41598-018-36918-8.
40. Walls AC, Tortorici MA, Snijder J, Xiong X, Bosch BJ, Rey FA, Veesler D. 2017. Tectonic conformational changes of a coronavirus spike glycoprotein promote membrane fusion. Proc Natl Acad Sci U S A 114: 11157–11162. https://doi.org/10.1073/pnas.1708727114.
41. Supekar VM, Bruckmann C, Ingallinella P, Bianchi E, Pessi A, Carfi A. 2004. Structure of a proteolytically resistant core from the severe acute respiratory syndrome coronavirus S2 fusion protein. Proc Natl Acad Sci U S A 101:17958–17963. https://doi.org/10.1073/pnas.0406128102.
42. Wu K, Chen L, Peng G, Zhou W, Pennell CA, Mansky LM, Geraghty RJ, Li F. 2011. A virus-binding hot spot on human angiotensin-converting enzyme 2 is critical for binding of two different coronaviruses. J Virol 85:5331–5337. https://doi.org/10.1128/JVI.02274-10.
43. Qian Z, Wang H, Empig C, Anderson WF, Albritton LM. 2004. Complementation of a binding-defective retrovirus by a host cell receptor mutant. J Virol 78:5766–5772. https://doi.org/10.1128/JVI.78.11.5766-5772.2004.
44. Di Giovine P, Settembre EC, Bhargava AK, Luftig MA, Lou H, Cohen GH, Eisenberg RJ, Krummenacher C, Carfi A. 2011. Structure of herpes simplex virus glycoprotein D bound to the human receptor nectin-1. PLoS Pathog 7:e1002277. https://doi.org/10.1371/journal.ppat.1002277.
45. Li W, Hulswit RJG, Widjaja I, Raj VS, McBride R, Peng W, Widagdo W, Tortorici MA, van Dieren B, Lang Y, van Lent JWM, Paulson JC, de Haan CAM, de Groot RJ, van Kuppeveld FJM, Haagmans BL, Bosch BJ. 2017. Identification of sialic acid-binding function for the Middle East respiratory syndrome coronavirus spike glycoprotein. Proc Natl Acad Sci U S A 114:E8508–E8517. https://doi.org/10.1073/pnas.1712592114.
46. Widagdo W, Okba NMA, Li W, de Jong A, de Swart RL, Begeman L, van den Brand JMA, Bosch BJ, Haagmans BL. 2019. Species-specific colocalization of Middle East respiratory system coronavirus attachment and entry receptors. J Virol 93:e00107-19. https://doi.org/10.1128/JVI.00107-19.